Applied Energy 348 (2023) 121531

Contents lists available at ScienceDirect

Applied Energy

journal homepage: www.elsevier.com/locate/apenergy

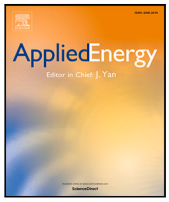

Increasing the lifetime profitability of battery energy storage systems through aging aware operation

Nils Collath [a,*], Martin Cornejo [a], Veronika Engwerth [a], Holger Hesse [b], Andreas Jossen [a]

[a] Technical University of Munich, TUM School of Engineering and Design, Department of Energy and Process Engineering, Chair of Electrical Energy Storage Technology, Arcisstr. 21, 80333 Munich, Germany

[b] Kempten University of Applied Sciences, Bahnhofstr. 61, 87435 Kempten, Germany

ARTICLE INFO

Keywords:
Battery energy storage system
Lithium-ion
Degradation model
Aging cost
Intraday trading
Energy arbitrage

ABSTRACT

Lithium-ion cells are subject to degradation due to a multitude of cell-internal aging effects, which can significantly influence the economics of battery energy storage systems (BESS). Since the rate of degradation depends on external stress factors such as the state-of-charge, charge/discharge-rate, and depth of cycle, it can be directly influenced through the operation strategy. In this contribution, we propose a model predictive control (MPC) framework for designing aging aware operation strategies. By simulating the entire BESS lifetime on a digital twin, different aging aware optimization models can be benchmarked and the optimal value for aging cost can be determined. In a case study, the application of generating profit through arbitrage trading on the EPEX SPOT intraday electricity market is investigated. For that, a linearized model for the calendar and cyclic capacity loss of a lithium iron phosphate cell is presented. The results show that using the MPC framework to determine the optimal aging cost can significantly increase the lifetime profitability of a BESS, compared to the prevalent approach of selecting aging cost based on the cost of the battery system. Furthermore, the lifetime profit from energy arbitrage can be increased by an additional 24.9% when using the linearized calendar degradation model and by 29.3% when using both the linearized calendar and cyclic degradation model, compared to an energy throughput based aging cost model. By examining price data from 2019 to 2022, the case study demonstrates that the recent increases in prices and price fluctuations on wholesale electricity markets have led to a substantial increase of the achievable lifetime profit.

1. Introduction

Stationary battery energy storage system (BESS) are used for a variety of applications and the globally installed capacity has increased steadily in recent years [1,2]. In behind-the-meter applications such as increasing photovoltaic self-consumption or optimizing electricity tariffs through peak shaving, BESSs generate cost savings for the end-user. In front-of-the-meter applications such as frequency regulation and energy arbitrage, operators generate revenue by marketing BESSs in the respective energy and power markets. Lastly, in microgrids using a BESS with a renewable energy source can be a cost-competitive option over relying on diesel generators [3].

Following the cost reductions and technological advances of recent years, lithium-ion cells are now the predominant battery technology for BESS installations [1,4]. However, like other battery types as well, lithium-ion batteries are subject to degradation due to a multitude of cell internal aging mechanisms. This leads, among others, to a decrease in cell capacity and an increase of the cell's internal resistance. Multiple reviews are available that focus on the aging mechanisms in lithium-ion cells [5–7].

On a system level, battery aging manifests itself in decreasing usable capacity and increasing charge/discharge losses over a BESS lifetime [8,9]. This in turn directly affects the economic viability of a BESS, as less profit from the application can be generated in later years compared to the beginning of life [10,11]. Furthermore, it is often assumed that after a certain extent of battery aging, the BESS will reach its end-of-life (EOL). A common assumption is to set the EOL to the point at which a certain level of remaining capacity, often named state of health [.] (SOH), is reached, for example at a SOH of 70% [12] or 80% [13–15] of the initial battery capacity. The physical rationale behind this assumption is that many lithium-ion cells show a rapid increase in their degradation rate following this SOH range, which is referred to as an aging knee or nonlinear aging [16,17]. In addition, manufacturers often provide warranties that cover batteries

* Corresponding author at: Technical University of Munich, TUM School of Engineering and Design, Department of Energy and Process Engineering, Chair of Electrical Energy Storage Technology, Arcisstr. 21, 80333 Munich, Germany.
E-mail address: nils.collath@tum.de (N. Collath).

https://doi.org/10.1016/j.apenergy.2023.121531
Received 4 April 2023; Received in revised form 13 June 2023; Accepted 25 June 2023
Available online 18 July 2023

Abbreviations

BESS	battery energy storage system
C_{rate}	charge-discharge rate
DOC	depth of cycle
EOL	end-of-life
FEC	full equivalent cycle
LFP	lithium iron phosphate
MILP	mixed integer linear programming
MPC	model predictive control
NPV	net present value
SimSES	Simulation Tool for Stationary Energy Storage Systems
SOC	state of charge
SOH	state of health [.]

General parameters

$\mathbb{C}^{aging}$	Total aging cost over the full optimization horizon [EUR]
$\mathbb{C}^{aging,cyc,cal}$	Total aging cost over the full optimization horizon for aging cost model (iii) [EUR]
$\mathbb{C}^{aging,FEC}$	Total aging cost over the full optimization horizon for aging cost model (i) [EUR]
$\mathbb{C}^{aging,FEC,cal}$	Total aging cost over the full optimization horizon for aging cost model (ii) [EUR]
$\mathbb{C}_t^{aging}$	Total aging cost in timestep t [EUR]
ΔFEC_t	Number of FECs in timestep t [.]
i	Interest rate [.]
$\mathbb{P}_m^{arb}$	Profit gained from energy arbitrage in year m [EUR]
$\mathbb{P}_t$	Profit gained in the respective application in timestep t [EUR]
SOH	state of health [.]

Optimization constants

η	Charge/discharge efficiency of the BESS assumed for the optimization model [.]
c^{aging}	Aging cost per unit of capacity loss for the optimization model [EUR/kWh]
c_t^{id}	Electricity price on the intraday electricity market in timestep t [EUR/kWh]
E^{batt}	Remaining rated energy after accounting for degradation [kWh]
E^n	Nominal battery capacity at the beginning of life [kWh]
$P^{AC,max}$	Maximum charge and discharge power of the BESS [kW]
$Q^{loss,cal}$	Total calendar capacity loss at the beginning of the optimization horizon [.]
$Q^{loss,cyc}$	Total cyclic capacity loss at the beginning of the optimization horizon [.]
X_i^{cal}	x-values of the linearized calendar aging function in point i [.]
X_j^{cyc}	x-values of the linearized cyclic aging function in point j [kWh]
Z_i^{cal}	z-values of the linearized calendar aging function in point i [.]
Z_j^{cyc}	z-values of the linearized cyclic aging function in point j [.]
Δt	Optimization timestep length [h]
FEC^{EOL}	Totals FECs until end-of-life is assumed [.]
SOC^{start}	SOC at the beginning of the optimization horizon [.]
SOH^{EOL}	SOH at which end-of-life is assumed [.]

Optimization index sets

H	Index set of timeblocks for the linearized cyclic aging model, $h \in H$
I	Index set of points for the linearized calendar aging model, $i \in I$
J	Index set of points for the linearized cyclic aging model, $j \in J$
T	Index set of timesteps for the current optimization horizon, $t \in T$
T_h	Index set of all timesteps in timeblock h, $t \in T_h$

Optimization decision variables

$\lambda_{t,i}^{cal}$	SOS-type 2 variables for linearization of calendar aging [.]
$\lambda_{h,j}^{cyc,ch}$	SOS-type 2 variables for linearization of cyclic aging in charge direction [.]
$\lambda_{h,j}^{cyc,dis}$	SOS-type 2 variables for linearization of cyclic aging in discharge direction [.]
e_h^{ch}	Energy throughput in charge direction in timeblock h [kWh]
e_h^{dis}	Energy throughput in discharge direction in timeblock h [kWh]
p_t^{ch}	Charge power of the BESS in timestep t [kW]
p_t^{dis}	Discharge power of the BESS in timestep t [kW]
$q_t^{loss,cal}$	Calendar capacity loss in timestep t [.]
$q_h^{loss,cyc,ch}$	Cyclic capacity loss in charge direction in timeblock h [.]
$q_h^{loss,cyc,dis}$	Cyclic capacity loss in discharge direction in timeblock h [.]
soc_t	BESS state-of-charge at timestep t [.]

dropping below a specified SOH threshold within the warranty period [18], which is why these thresholds can act as a reference for the techno-economic assessment and operation of BESSs.

The rate of battery aging itself depends on multiple external stress factors [19], which enables the operator to influence the aging behavior through the operating conditions. For the purpose of BESS operation, battery aging can be grouped into calendar and cyclic aging. Calendar aging refers to those mechanisms that occur regardless of the battery being cycled or not, for example the continued growth of the solid electrolyte interphase [19]. Calendar aging generally progresses faster at a high storage temperature and a high state of charge (SOC) [20,21]. Cyclic aging refers to those aging mechanisms that occur as a consequence of cycling the battery cells, such as particle cracking, solid electrolyte interphase re-formation at newly exposed anode surface areas, and lithium plating [19]. Cyclic aging progresses with the growing number of charge/discharge cycles and tends to accelerate when cycling at a high charge-discharge rate (C_{rate}) and a high depth of cycle (DOC) [22,23]. In addition, both high and low temperatures [23] and cycling a battery in particularly straining SOC ranges can accelerate cyclic aging [20].

Operating a BESS under consideration of the relevant stress factors provides an opportunity to slow down battery aging. Aging aware operation therefore promises higher profits over the BESS lifetime and more resource-efficient use of the battery cells. In this contribution, we propose a model predictive control (MPC) framework for aging

aware operation of BESSs. The MPC framework allows benchmarking the performance of different aging aware optimization models on a digital twin of a BESS. Thereby, the operation strategy can be designed and validated before being deployed on the real-world BESS. While we focus on the application of energy arbitrage, the framework is transferable to other applications as well. In the following two subsections of this introduction, we will first present the literature review before describing the structure and highlighting the main contributions of this work.

1.1. Literature review

The process of deriving a series of charge and discharge signals for a BESS under consideration of technical constraints and economic benefit is referred to with different terms in the literature: operation strategy [24], energy management [25], scheduling [26], control [27], or dispatch [28]. We here refer to this process as an operation strategy in the following. A distinction is then made between simple, rule-based operation strategies and optimization-based operation strategies, which also differ in how battery aging can be incorporated, i.e. how the operation strategy can be made "aging aware" [10]. Examples of rule-based, aging aware operation strategies are variable limits for the maximum C_{rate} of the BESS [29], or forecast-based rules such as to only charge a home-storage system with the amount of surplus photovoltaic energy during the day, that is forecasted to be needed during the night, thereby reducing calendar aging [24].

Optimization-based operation strategies generally aim to find an optimum to an objective function, which is also referred to as a fitting or reward function for some methods. The methods used to determine the optimum can be classified into exact solution approaches (e.g. linear programming), heuristics (e.g. reinforcement learning), and meta-heuristics (e.g. particle swarm optimization) [25]. A particularly common approach for considering battery aging in an optimization-based operation strategy is to define a monetary value that represents the effects of battery aging, i.e. aging cost [19]. This approach allows to link the short-term scheduling problem to long-term degradation effects:

$$\max \sum_{t \in T} \left(\mathbb{P}_t - \mathbb{C}_t^{\text{aging}} \right) \tag{1}$$

Here, $\mathbb{P}_t$ is the profit gained in the respective application for timestep $t \in T$ and $\mathbb{C}_t^{\text{aging}}$ the total aging cost for timestep $t \in T$. The total aging cost $\mathbb{C}_t^{\text{aging}}$ is then either calculated based on each percentage point of SOH loss in each time step ΔSOH_t as in Eq. (2) [12–15,28] or based on the number of full equivalent cycles (FECs) in each time step ΔFEC_t as in Eq. (3) [30–34].

$$\mathbb{C}_t^{\text{aging,SOH}_t} = \frac{c^{\text{aging}} \cdot E^{\text{n}}}{1 - \text{SOH}^{\text{EOL}}} \cdot \Delta\text{SOH}_t \tag{2}$$

$$\mathbb{C}_t^{\text{aging,FEC}} = \frac{c^{\text{aging}} \cdot E^{\text{n}}}{\text{FEC}^{\text{EOL}}} \cdot \Delta\text{FEC}_t \tag{3}$$

Here, SOH^{EOL} and FEC^{EOL} represent the SOH threshold and number of FECs after which the EOL of the battery is reached. E^n is the nominal battery capacity at the beginning of life in kWh. The aging cost c^{aging} in EUR per kWh is then typically set to a cost value that relates to the battery system, such as the full storage system investment cost [14,33,34], battery investment cost [11,35,36], battery replacement cost [12,15,37], battery cell replacement cost [13,30], or generic battery cost [28,31,38].

This common practice of setting the value of aging cost c^{aging} equal to battery system cost has a shortcoming: The profit generated in a given application, e.g. performing energy arbitrage through an electricity exchange, is generated after the BESS has been installed and has no dependence on the original system cost. Instead, c^{aging} can be seen as a penalty factor for operating a BESS. As we will show, by using the proposed MPC framework to determine the optimal value for c^{aging} based on the application and battery aging behavior, a higher lifetime profitability can be achieved.

Furthermore, different approaches are found in the literature for modeling battery aging as part of the optimization problem. The different degradation modeling approaches vary in their degree of complexity and the solution methods required to solve the resulting optimization problem. In relation to Eqs. (2) and (3), these degradation models are additional constraints that define how ΔSOH_t and FEC^{EOL} are calculated based on the operating conditions.

Table 1 shows an overview of related publications that propose aging aware operations strategies for energy arbitrage with BESSs. Hesse et al. [28] and Kumtepeli et al. [39] both used semi-empirical degradation models as part of their mixed integer linear programming (MILP) optimization, the originally nonlinear, calendar and cyclic degradation models were linearized in order to be solved in the MILPs. Englberger et al. used an MPC approach, in which no other stress factors than the charge throughput are considered in the optimization model, but a separate nonlinear, semi-empirical degradation model is run to validate the optimization results and update the SOH [34]. Cao et al. used a reinforcement learning approach in which a reinforcement learning agent is trained on both predictions and a nonlinear battery model that accounts for calendar and cyclic capacity loss [38]. Reniers et al. compared three different degradation models with a sliding horizon optimization over a one-year timeframe, the most complex model being a single particle physicochemical model, which required a complex gradient-based nonlinear solution approach to solve [27].

Optimization models for BESS operation can get complex and timely to solve even without incorporating battery aging, for example when using stochastic programming to consider forecast uncertainty or when optimizing for multi-use applications, in which multiple applications are served by the same BESS [40]. The question that remains is what benefit can be gained by using more complex degradation models as part of the optimization model when considering the entire BESS lifetime. This requires the determination of the lifetime optimal aging cost of each model for a fair comparison. Maheshwari et al. used different weighting factors which are to be set by the operator to link aging cost to the profit from the application and investigated only a 1-week timeframe [41]. He et al. notably proposed an optimization model that determines the optimal aging cost value [42]. The optimization model however, includes a simplified aging model that only accounts for the DOC dependence of cyclic aging.

In contrast to previous contributions, the MPC framework proposed here allows the comparison of different optimization models on a digital twin of a BESS. By finding the optimal aging cost value c^{aging} for each optimization model and by considering the entire BESS lifetime, the optimal lifetime profit of different aging aware operation strategies can be quantified. Thereby, the proposed MPC framework can be used to benchmark different aging aware operation strategies on a digital twin, before deploying the optimal strategy on the real-world BESS.

1.2. Structure and main contributions

In the following sections, we first describe the proposed MPC framework. In addition, the electricity price time series used for the case study, the different aging aware optimization models, and the software that is used as a digital twin of the BESS are presented. In the subsequent case study, the application of energy arbitrage on the intraday electricity market is investigated. We thereby showcase the functionality of the MPC framework and investigate the increase in lifetime profitability that can be achieved by determining the optimal aging cost value and by using different degrees of complexity for modeling battery aging as part of the optimization model. We summarize our main contributions as follows:

- Open-source MPC framework for designing aging aware operation strategies on a digital twin of a BESS

Table 1
Publications that propose aging aware operation strategies for energy arbitrage with BESSs, compared to this contribution.

Reference	Stress factors considered in optimization model	Optimal aging cost	Investigated timeframe	MPC approach
Kazemi[a] [37]	$Q^{\mathrm{loss,cyc}}(\mathrm{FEC}, \mathrm{DOC})$	no (c^{aging}: replacement cost)	1 day	no
Hesse [28]	$Q^{\mathrm{loss,cal}}(t, \mathrm{SOC})$; $Q^{\mathrm{loss,cyc}}(\mathrm{FEC}, \mathrm{C_{rate}})$	no (c^{aging}: battery cost)	1 month	no
Reniers [27]	Various (physicochemical model)	no (c^{aging}: battery cost)	1 week	no
Cao[a] [38]	$Q^{\mathrm{loss,cal}}(t, \mathrm{SOC}, T)$; $Q^{\mathrm{loss,cyc}}(\mathrm{FEC}, \mathrm{DOC}, \overline{\mathrm{SOC}}, T)$[a]	no (c^{aging}: battery cost)	1 year	no
Maheshwari [41]	$Q^{\mathrm{loss,cyc}}(\mathrm{FEC}, \mathrm{DOC}, \overline{\mathrm{SOC}}, \mathrm{C_{rate}})$	no (c^{aging}: weighting factors)	7 days	no
Wankmuller [9]	$Q^{\mathrm{loss,cyc}}(\mathrm{FEC})$	no (c^{aging}: different values)	10 years	no
He [42]	$Q^{\mathrm{loss,cyc}}(\mathrm{FEC}, \mathrm{DOC})$	**yes**	**full lifetime**	no
Englberger[a] [34]	$Q^{\mathrm{loss,cyc}}(\mathrm{FEC})$	no (c^{aging}: battery cost)	**full lifetime**	partially
Kumtepeli [39]	$Q^{\mathrm{loss,cal}}(t, \mathrm{SOC}, T)$; $Q^{\mathrm{loss,cyc}}(\mathrm{FEC}, \mathrm{C_{rate}}, T)$	no (c^{aging}: battery cost)	1 year	**yes**
This contribution	$Q^{\mathrm{loss,cal}}(t, \mathrm{SOC})$; $Q^{\mathrm{loss,cyc}}(\mathrm{FEC}, \mathrm{DOC}, \mathrm{C_{rate}})$	**yes**	**full lifetime**	**yes**

[a]Kazemi et al. consider frequency regulation in addition to energy arbitrage while Englberger et al. consider energy arbitrage, frequency regulation and peak shaving. In Cao et al. the stress factors are not explicitly considered in the operation strategy, but the reinforcement learning agent is trained on a battery model that considers these stated stress factors.

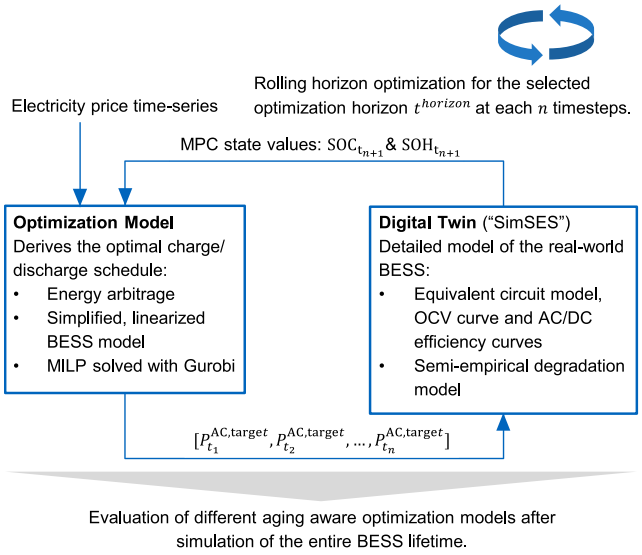

Fig. 1. Depiction of the proposed MPC framework for designing and validating aging aware operation strategies. Our implementation of the MPC framework is available open-source under [43].

- Linearized lithium iron phosphate (LFP) cell degradation models, suitable for MILP
- Increased lifetime profitability through determining the *optimal aging cost*, thereby optimizing both short-term profit and long-term degradation effects
- Quantification of the increase in lifetime profitability through aging aware operation with different levels of degradation model complexity
- Analysis of factors influencing the *optimal aging cost*: interest rate, EOL-criterion, and intraday electricity price (2019 to 2022)
- A formulation for aging cost that accounts for the interest rate

2. Model predictive control framework for designing aging aware operation strategies

The proposed MPC framework is shown in Fig. 1. The digital twin is a detailed model of the investigated BESS and should represent the real-world BESS and its expected aging behavior accurately. We use the in-house developed, open-source Simulation Tool for Stationary Energy Storage Systems (**SimSES**) as the digital twin, which is described in detail in [44]. Optimization models have limitations in their complexity determined by the optimization method that is used. For example, linear programming requires a linear objective function and constraints, while quadratic programming also allows quadratic objective functions. Generally, the optimization model will therefore incorporate a simplified storage model, which in turn is a simplified version of the digital twin.

The optimization model is solved for the selected optimization horizon t^{horizon} with a time resolution of Δt, after which the resulting power targets $P^{\mathrm{AC,target}}$ for the next n timesteps are simulated with the digital twin. For $n = 1$, the optimization model is solved at every timestep and only the power target for the next timestep is passed to the simulation model before the next optimization is called. The relevant MPC state values, that represent the new BESS state after these n timesteps, are handed back to the optimization model to solve the next optimization horizon. Thereby the more accurate digital twin is used to validate the operation strategy derived through the optimization model. Also, this framework mirrors the real-world application, where the operation strategy would be run in a similar MPC approach on a real BESS instead of the digital twin.

The relevant MPC state values of the digital twin used in this contribution are the SOC and the capacity-based SOH, but further values could be used for the optimization model such as the system temperature. Our implementation of the proposed MPC framework is available open-source [43] and designed in a modular way, such that different use cases or optimization formulations can be added and investigated. Here, we focus on the application of energy arbitrage on the European intraday spot market. In the following, we will first describe the electricity price time series, before presenting the digital twin model and the investigated optimization models.

2.1. Price time series

We investigate the application of generating profit through arbitrage trading on the intraday electricity market. For that, we use data from the largest European intraday power exchange, the EPEX SPOT, with price data obtained from [45]. The intraday electricity prices are shown in Fig. 2. Price data from the year 2021 serves as the base scenario in the later case study. Since the intraday market is designed to offer continuous trading, not one fixed price exists for a given delivery period. The ID-1 price index is the weighted price average off all trades executed within 1 h before delivery [46]. Because this index represents the potential to market flexibility without inflating optimistic price assumptions, it has been used as a benchmark in previous publications to develop and test energy arbitrage strategies [47] and is also adopted for the later case study presented here. While the average ID-1 price for the year 2021 is at 97.15 EUR/MWh, individual price peaks of up to 942.35 EUR/MWh and down to −122.92 EUR/MWh are found in the data.

2.2. Digital twin

SimSES allows to conduct time series based simulations for stationary energy storage systems and includes equivalent circuit models and degradation models for different battery systems [44]. It also includes models for periphery components such as the AC/DC converter. For

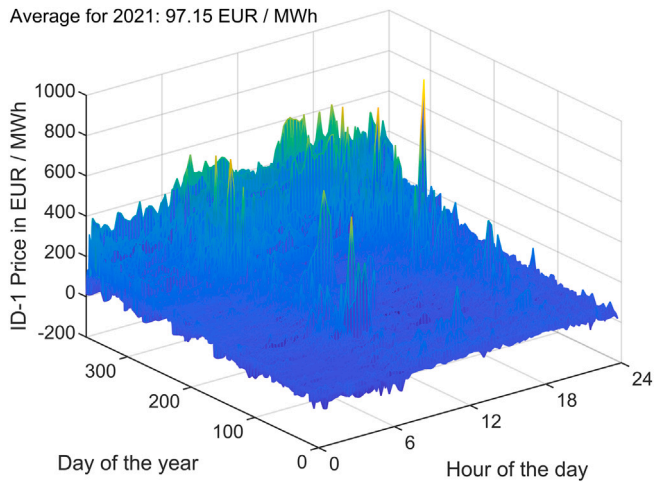

Fig. 2. 15 min Intraday ID-1 electricity prices for the year 2021 with data obtained from [45].

Table 2
Key parameters for the digital twin in **SimSES**.

Parameter	Value
Cell type	Sony/Murata LFP-graphite
Degradation model	Semi-empirical by Naumann et al. [48,49]
AC/DC converter	Notton et al. [50]
System sizing	1 MW, 1.2 MWh

the cell model, we use a model of a Sony/Murata LFP graphite cell for which a semi-empirical degradation model by Naumann et al. has been incorporated into **SimSES** [48,49]. For the AC/DC converter, an efficiency curve by Notton et al. is used [50]. Table 2 summarizes the key parameters.

2.3. Optimization models

We investigate the increase in lifetime profitability achieved through different degrees of complexity for modeling battery aging as part of the optimization model. All three optimization model types are formulated as either linear programs or mixed integer linear programs and structured as follows:

$$\max \sum_{t\in T} \left((p_t^{\mathrm{dis}} - p_t^{\mathrm{ch}}) \cdot \Delta t \cdot c_t^{\mathrm{id}} \right) - \mathbb{C}^{\mathrm{aging}} \tag{4}$$

The first part of the equation is the profit generated on the intraday market. Here, p_t^{dis} and p_t^{ch} are the discharged and charged power of the BESS and c_t^{id} the electricity price on the intraday electricity market at time t. Δt is the optimization timestep, which is set to 15 min. $\mathbb{C}^{\mathrm{aging}}$ is the total aging cost over the optimization horizon. In addition to the objective function, the constraints below ensure energy conservation and provide upper and lower limits for the three sets of continuous decision variables, p_t^{dis}, p_t^{ch}, and soc_t with $t \in T$:

$$soc_t = soc_{t-1} + \frac{\Delta t}{E^{\mathrm{batt}}} \cdot \left(p_t^{\mathrm{ch}} \eta - \frac{1}{\eta} p_t^{\mathrm{dis}} \right) \quad \forall\, t \in T \backslash \{0\} \tag{5}$$

$$soc_{t=0} = \mathrm{SOC}^{\mathrm{start}} + \frac{\Delta t}{E^{\mathrm{batt}}} \cdot \left(p_{t=0}^{\mathrm{ch}} \eta - \frac{1}{\eta} p_{t=0}^{\mathrm{dis}} \right) \tag{6}$$

$$0 \le p_t^{\mathrm{ch}}, p_t^{\mathrm{dis}} \le P^{\mathrm{AC,max}} \quad \forall\, t \in T \tag{7}$$

$$0 \le soc_t \le 1 \quad \forall\, t \in T \tag{8}$$

$\mathrm{SOC}^{\mathrm{start}}$ and E^{batt} are the SOC at the beginning of the optimization horizon and the remaining rated energy of the BESS after accounting for degradation, respectively. $P^{\mathrm{AC,max}}$ is the maximum charge and discharge power of 1 MW. soc_t is the energy based state of charge of the BESS at every time step and η the fixed charge/discharge efficiency.

Notably, one could use a linearized model for the efficiency that follows the BESS efficiency curve [14,28] instead of a constant for η We found good results with a constant efficiency factor of $\eta = 0.9$ and focus here on modeling of battery aging in the optimization model. However, the system model in **SimSES** as part of the MPC framework models power losses in both the battery cells through the battery cell internal resistance and the AC/DC converter through an efficiency curve.

For the total aging cost $\mathbb{C}^{\mathrm{aging}}$, we investigate different models with increasing complexity that are described in the following subsections.

2.3.1. Aging cost model (i) - Energy throughput

This aging cost model defines aging cost based on the energy throughput of the BESS and the expected amount of FECs the system can endure before reaching its EOL. This model does not explicitly consider any other stress factors of either calendar or cyclic aging. The aging cost $\mathbb{C}^{\mathrm{aging,FEC}}$ are defined as follows:

$$\begin{aligned} \mathbb{C}^{\mathrm{aging,FEC}} &= \sum_{t\in T} \frac{(p_t^{\mathrm{ch}} + p_t^{\mathrm{dis}}) \cdot \Delta t}{E^{\mathrm{n}} \cdot 2} \cdot \frac{E^{\mathrm{n}} \cdot c^{\mathrm{aging}}}{\mathrm{FEC}^{\mathrm{EOL}}} \\ &= \sum_{t\in T} \frac{(p_t^{\mathrm{ch}} + p_t^{\mathrm{dis}}) \cdot \Delta t \cdot c^{\mathrm{aging}}}{2 \cdot \mathrm{FEC}^{\mathrm{EOL}}} \end{aligned} \tag{9}$$

The first part of the top equation denotes the change in FECs, based on the charge and discharge power, p_t^{ch} and p_t^{dis}, in the given timestep, the timestep width Δt and the rated energy of the BESS at the beginning of life E^n. The second part expresses the aging cost per FEC, based on the aging cost per kWh c^{aging} and the expected number of cycles until EOL $\mathrm{FEC}^{\mathrm{EOL}}$.

We here set $\mathrm{FEC}^{\mathrm{EOL}} = 6000$, as the 80% SOH limit is reached after 6000 FECs for the majority of cycling conditions in the LFP cell aging study [49]. How to determine the optimal value for the aging cost c^{aging} will be investigated in the later case study. This aging cost model equals the common definition from Eq. (3), with a fixed value for $\mathrm{FEC}^{\mathrm{EOL}}$.

2.3.2. Aging cost model (ii) — Energy throughput and calendar degradation model

In addition to the energy throughput model, a linearized version of the calendar degradation model from Naumann et al. [48] is implemented in the optimization model. Thereby, this aging cost model with the aging cost $\mathbb{C}^{\mathrm{aging,FEC,cal}}$ accounts for the SOC dependence of calendar aging in the optimization:

$$\begin{aligned} \mathbb{C}^{\mathrm{aging,FEC,cal}} =& \mathbb{C}^{\mathrm{aging,FEC}} \\ &+ \sum_{t\in T} \frac{E^{\mathrm{batt}}}{1 - \mathrm{SOH}^{\mathrm{EOL}}} \cdot c^{\mathrm{aging}} \cdot q_t^{\mathrm{loss,cal}} \end{aligned} \tag{10}$$

$\mathbb{C}^{\mathrm{aging,FEC}}$ is the definition of energy throughput based aging cost from Eq. (9). $\mathrm{SOH}^{\mathrm{EOL}}$ is the SOH threshold at which the EOL is defined and $q_t^{\mathrm{loss,cal}}$ is the projected calendar capacity loss in the given timestep in per unit as a continuous decision variable.

The calendar degradation model from Naumann et al. [48] is linearized as detailed in Appendix A such that it can be solved as part of a MILP. The resulting linearization is depicted in Fig. 3 and implemented in the optimization model as below:

$$\sum_{i\in I} \lambda_{t,i}^{\mathrm{cal}} \cdot X_i^{\mathrm{cal}} = soc_t \quad \forall\, t \in T \tag{11}$$

$$\sum_{i\in I} \lambda_{t,i}^{\mathrm{cal}} \cdot Z_i^{\mathrm{cal}} = q_t^{\mathrm{loss,cal}} \quad \forall\, t \in T \tag{12}$$

$$\sum_{i\in I} \lambda_{t,i}^{\mathrm{cal}} = 1 \quad \forall\, t \in T \tag{13}$$

I is the set of points used for the linearization of the calendar aging function. X_i^{cal} with $i \in I$ are the x-values of the linearization from Fig. 3, representing the SOC. Z_i^{cal} with $i \in I$ are the z-values of the linearization from Fig. 3, meaning the calendar capacity loss in a given

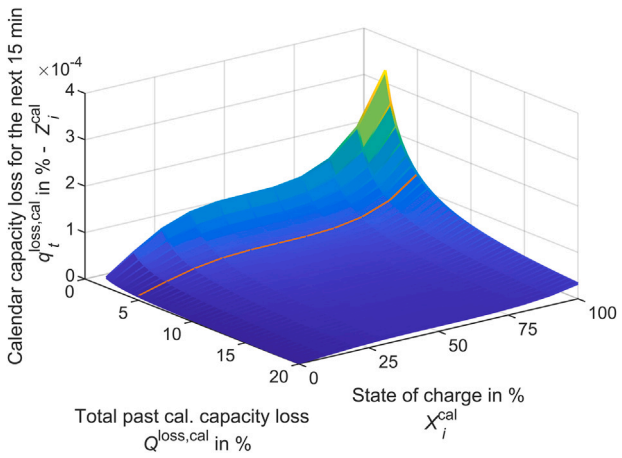

Fig. 3. Linearized calendar degradation model. A set of 10 lines is used to represent the SOC dependency of calendar aging. To account for the dependence of future degradation on the total past capacity loss $Q^{loss,cal}$, a lookup table with 229 sets of these 10 lines is used, such that the correct set of lines can be chosen at the beginning of the optimization horizon based on $Q^{loss,cal}$. However, $Q^{loss,cal} = 5\%$ (marked in orange) serves as the base scenario for the optimization.

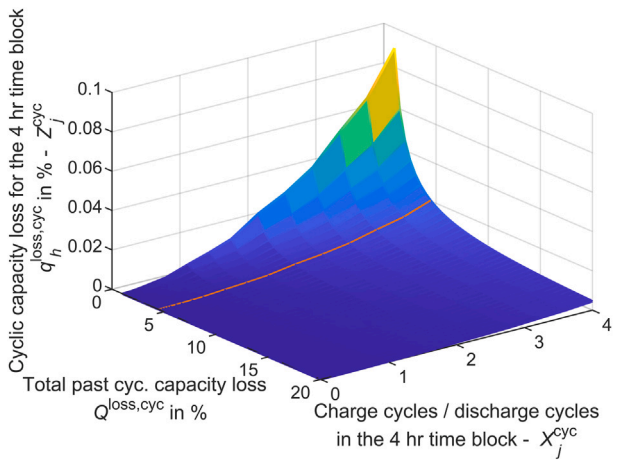

Fig. 4. Linearized cyclic degradation model. A set of 27 lines is used to represent the amount of cyclic degradation for a given 4 h time block, based on the number of charge cycles or discharge cycles in that time block. To account for the dependence of future degradation on the past total cyclic capacity loss $Q^{loss,cyc}$, a lookup table with 229 sets of these 27 lines is used, such that the correct set of lines can be chosen at the beginning of each optimization based $Q^{loss,cyc}$. However, $Q^{loss,cyc} = 5\%$ (marked in orange) serves as the base scenario for the optimization.

15 min timestep for the respective SOC. $\lambda_{t,i}^{cal}$ $\lambda_{t,i}^{cal}$ with $t \in T$ and $i \in I$ each are continuous variables that are used to represent the linearized calendar aging function in the optimization model. The set of variables $\lambda_{t,i}^{cal}$ with $i \in I$ is implemented as one special ordered set of type 2 for each $t \in T$. This means that at most two variables of each set can be nonzero, and they must be consecutive in their ordering. In addition, the following constraints for the decision variable $q_t^{loss,cal}$ and $\lambda_{t,i}^{cal}$ are implemented:

$$0 \leq q_t^{loss,cal} \quad \forall\, t \in T \tag{14}$$

$$0 \leq \lambda_{t,i}^{cal} \leq 1 \quad \forall\, t \in T,\ \forall\, i \in I \tag{15}$$

As Fig. 3 shows, calendar aging has a square root dependence on past capacity loss due to the $\sqrt{t}$ dependence of the original calendar aging function. Multiple other calendar degradation models have this sublinear dependency of calendar capacity loss on time as well [51], which some authors also implement in the optimization model [13]. However, as we will show in the case study, implementing this dependency in the optimization would lead to sub-optimal lifetime profit of the BESS, as calendar aging cost would be significantly higher in earlier than in later years of operation. Therefore, we choose the linearization at $Q^{loss,cal} = 5\%$ as the base scenario in the later case study, which is marked with an orange line in Fig. 3.

2.3.3. Aging cost model (iii) — Cyclic and calendar degradation model

Here, the calendar degradation model [48] and cyclic degradation model [49] are both linearized and implemented in the optimization model. The aging cost model thereby accounts for the stress factors of both calendar and cyclic aging. The linearization is described in detail in Appendix A. The resulting definition for the aging cost $\mathbb{C}^{aging,cyc,cal}$ is as follows:

$$\mathbb{C}^{aging,cyc,cal} = \frac{E^{batt}}{1 - SOH^{EOL}} \cdot c^{aging} \cdot \Big(\sum_{t \in T} q_t^{loss,cal} + \sum_{h \in H} \big(q_h^{loss,cyc,ch} + q_h^{loss,cyc,dis} \big) \Big) \tag{16}$$

The objective function includes the calendar aging cost from Eq. (10) of the previous subsection. The previous constraints Eqs. (13) to (14) are included in this model as well.

The linearized cyclic degradation model is split in the cyclic capacity loss in charge and cyclic capacity loss in discharge direction, i.e. $q_h^{loss,cyc,ch}$ and $q_h^{loss,cyc,dis}$. As described in Appendix A, cyclic aging is calculated separately for every 4 h time horizon h in the optimization horizon $h \in H$. This means for a 12 h optimization horizon, H would be an index set of three elements. For each of these 4 h time blocks, the total energy throughput in charge direction e_h^{ch} and discharge direction e_h^{dis} are calculated:

$$\sum_{t \in T_h} p_t^{ch} \cdot \Delta t = e_h^{ch} \quad \forall\, h \in H \tag{17}$$

$$\sum_{t \in T_h} p_t^{dis} \cdot \Delta t = e_h^{dis} \quad \forall\, h \in H \tag{18}$$

Here, T_h is the set of all timesteps in each of the 4 h time blocks. Based on this energy throughput, the cyclic aging for each 4 h time block is calculated with the linearized cyclic degradation model, analogously to the calendar degradation model from the previous subsection:

$$\sum_{j \in J} \lambda_{h,j}^{cyc,ch} \cdot X_j^{cyc} = e_h^{ch} \quad \forall\, h \in H \tag{19}$$

$$\sum_{j \in J} \lambda_{h,j}^{cyc,dis} \cdot X_j^{cyc} = e_h^{dis} \quad \forall\, h \in H \tag{20}$$

$$\sum_{j \in J} \lambda_{h,j}^{cyc,ch} \cdot Z_i^{cyc} = q_h^{loss,cyc,ch} \quad \forall\, h \in H \tag{21}$$

$$\sum_{j \in J} \lambda_{h,j}^{cyc,dis} \cdot Z_i^{cyc} = q_h^{loss,cyc,dis} \quad \forall\, h \in H \tag{22}$$

$$\sum_{j \in J} \lambda_{h,j}^{cyc,ch} = 1 \quad \forall\, h \in H \tag{23}$$

$$\sum_{j \in J} \lambda_{h,j}^{cyc,dis} = 1 \quad \forall\, h \in H \tag{24}$$

J is the set of points used for the linearization of the cyclic aging function. X_j^{cyc} with $j \in J$ are the x-values of the linearization from Fig. 4, representing the energy throughput for a 4 h time block. Z_j^{cyc} are the z-values of the linearization from Fig. 4, meaning the cyclic capacity loss for a 4 h time block in p.u. for the respective energy throughput. The sets of continuous variables $\lambda_{h,j}^{cyc,ch}$ and $\lambda_{h,j}^{cyc,dis}$ with $j \in J$ are implemented as special ordered sets of type 2 for each $h \in H$. In addition, the following constraints for the continuous decision variables $\lambda_{h,j}^{cyc,ch}$, $\lambda_{h,j}^{cyc,dis}$, $q_h^{loss,cyc,ch}$, $q_h^{loss,cyc,dis}$, e_h^{ch} and e_h^{dis} are implemented:

$$0 \leq \lambda_{h,j}^{cyc,ch}, \lambda_{h,j}^{cyc,dis} \leq 1 \quad \forall\, h \in H,\ \forall\, j \in J \tag{25}$$

$$0 \leq q_h^{\text{loss,cyc,ch}}, q_h^{\text{loss,cyc,dis}}, e_h^{\text{ch}}, e_h^{\text{dis}} \quad \forall\, h \in H \tag{26}$$

Analogously to the calendar degradation model, the cyclic degradation model has a square root dependence on past cyclic capacity loss due to the square root dependence of the original cyclic aging function on the number of FECs, see Fig. 4. As we will highlight in the case study, implementing this sublinear relationship in the optimization model would lead to sub-optimal lifetime profit of the BESS as well, since the cyclic aging cost would be significantly higher in earlier than in later years of operation. Therefore, we choose the linearization at $Q^{\text{loss,cyc}} = 5\%$ as the base scenario in the later case study, which is marked with an orange line in Fig. 4.

3. Simulation case study

In this chapter, we present and discuss the simulation results with the proposed MPC simulation framework. Section 3.1 shows the dependence of the lifetime cumulative arbitrage profit on the selection of the aging cost c^{aging} and highlights the increase in lifetime profitability that can be achieved by finding the optimal value for c^{aging}, i.e. the *optimal aging cost*. In Section 3.2, we investigate the benefits of the different aging cost model types. In Section 3.3, we show that the interest rate, EOL criterion, and the price time series all affect the *optimal aging cost*. Furthermore, Section 3.3 will highlight that the common practice of defining battery aging cost based on the cost of the battery system (c.f. Section 1.1) leads to reduced lifetime arbitrage profit, as opposed to using the here proposed MPC simulation framework to find the *optimal aging cost*. Section 3.4 proposes a novel definition of aging cost that promises higher economic return by accounting for the interest rate.

In the following, the optimization models use a time horizon t^{horizon} of 12 hr, with a timestep Δt of 15 min. For aging cost model type (i), the optimization is called every 30 min ($n = 2$) and for aging cost model type (ii) and type (iii) every 60 min ($n = 4$). The digital twin in **SimSES** in all cases runs on a 3 min time resolution. The commercial solver Gurobi Optimizer is used for solving the optimization models. Note that the resulting optimization problem for cost model type (i) is a linear program, while the special ordered sets in aging cost model type (ii) and (iii) require a MILP solver. The simulations for the case study were run on a workstation with an Intel Xeon W-2265 CPU and 96 GB RAM with multiple simulations in parallel. Running one year of simulation with the complete MPC framework took on average 23.4 min with aging cost model type (i), 73.6 min with model type (ii), and 308.7 min with model type (iii). Fig. 5 shows one exemplary day of operation with the three different aging cost models. In general, the profit in the energy arbitrage application is generated by charging at low prices and discharging at high prices. However, the different implementations of aging costs lead to different schedules. Aging cost model type (i) has aging costs that only depend on the energy throughput and do not explicitly consider any other aging stress factors, which results in the BESS charging up early at a low ID-1 price. Implementing the SOC dependence of calendar aging for model type (ii) results in the BESS charging later and discharging earlier to keep the SOC low. The added dependence of cyclic aging on DOC and C_{rate} for model type (iii) entices more shallow cycles at low DOC and C_{rate}, such as for the small price changes at 00:45 and 17:00 in Fig. 5.

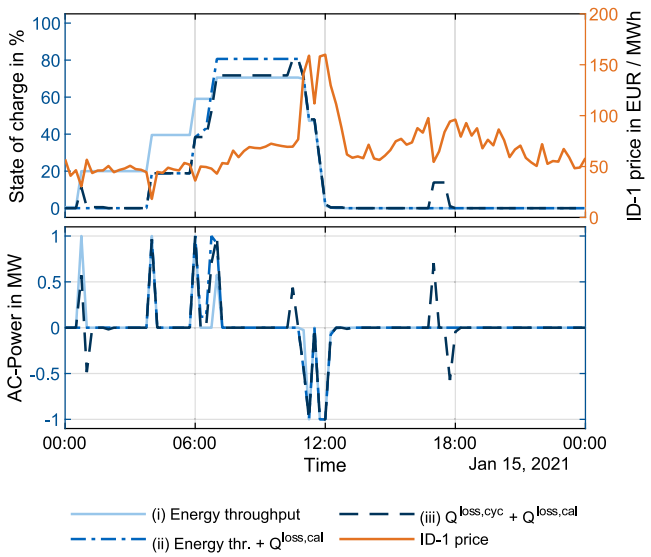

Fig. 5. One exemplary day of operation with the three different aging cost models.

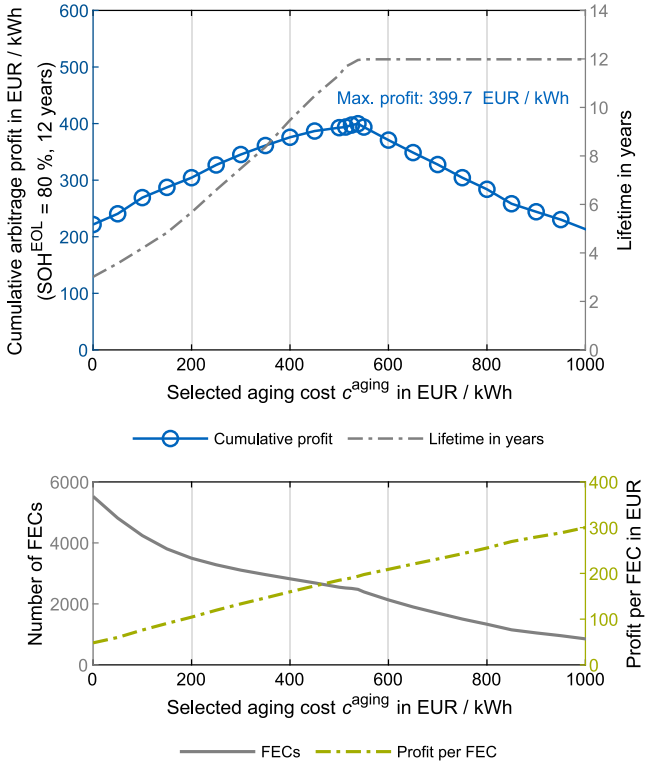

Fig. 6. Top: Cumulative profit from energy arbitrage and lifetime in years after 12 years of operation for different aging cost values. The profit is stated in EUR/kWh with regards to the initial nominal capacity ($E^{\text{n}} = 1.2$ MWh). Here, aging cost model (i) is used, i.e. the energy throughput model. The maximum cumulative profit is obtained if aging costs are defined such that the EOL criterion is reached at the end of the investigated 12-year horizon and an *optimal aging cost* of $c^{\text{aging}} = 538$ EUR/kWh. Bottom: FECs and profit per FEC for the different aging cost values.

3.1. Increased lifetime profit through the optimal choice of aging cost

To investigate the effect of aging cost c^{aging} on the lifetime profit from energy arbitrage, multiple 12-year simulations with different aging cost values were conducted. Fig. 6 shows the resulting cumulative profit and number of FECs for aging cost model (i), i.e. the energy throughput model. The cumulative profit includes the gains and losses from energy arbitrage, but no BESS investment cost. It therefore reflects the profit gained in the application, which after installation of the BESS is independent of the initial investment cost. The 12-year time horizon is chosen arbitrarily to reflect an investor's goal of achieving maximum profit over a fixed timeframe of interest, and will be varied in the later subsections.

The top of Fig. 6 shows the benefit of finding the *optimal aging cost*. If c^{aging} is chosen lower than optimal, the high amount of cycling will cause the BESS to degrade quickly and reach its EOL before the end of the 12-year time horizon. With aging cost of 0 EUR/kWh, the BESS

reaches its EOL at 80% SOH after 3.0 years and 5525.7 FECs, while obtaining a cumulative profit of 265.9 kEUR, or 221.6 EUR/kWh with regards to the initial nominal capacity of 1.2 MWh. If c^{aging} is chosen higher than optimal, the low amount of cycling will cause the BESS to forego energy arbitrage opportunities, leading to lower profit over the 12-year time horizon. With aging cost of 1000 EUR/kWh, the BESS obtains a cumulative profit of 256.1 kEUR or 213.4 EUR/kWh through energy arbitrage after only 852.8 FECs over the 12 years, while still having a remaining SOH of 86.7%. The highest cumulative profit is obtained if aging cost are chosen such that the EOL threshold of 80% remaining capacity is reached at the end of the investigated 12-year time horizon. With the *optimal aging cost* of c^{aging} = 538 EUR/kWh, the BESS generates a cumulative profit from energy arbitrage of 479.7 kEUR or 399.7 EUR/kWh, while reaching its EOL at the end of the 12-year time horizon after 2476.7 FECs.

The bottom part of Fig. 6 highlights the diminishing marginal return of additional cycles. When setting the aging cost to a high value, only the most profitable energy arbitrage opportunities are part of the optimization model's solution, resulting in a profit per FEC of 300.3 EUR for aging cost of 1000 EUR/kWh. On the other side, low aging cost lead to a high amount of cycles and even less profitable energy arbitrage opportunities being part the optimization model's solution, with a profit per FEC of 48.1 EUR for aging cost of 0 EUR/kWh.

3.2. Increased lifetime profit through advanced aging cost models

In this section, we investigate the benefit of the previously presented aging cost models. The top of Fig. 7 shows the cumulative profit after 12 years for all three previously introduced aging cost models with increasing complexity. In all three cases, the digital twin in **SimSES** as well as the price time series remain the same and only the optimization model formulation changes. Since the modeling approach differs between the aging cost models, different *optimal aging cost* lead to the maximum arbitrage profit when considering the entire BESS lifetime: c^{aging} = 538 EUR/kWh for model type (i) with only energy throughput being considered, c^{aging} = 275 EUR/kWh for model type (ii) with energy throughput and the linearized calendar degradation model, and c^{aging} = 350 EUR/kWh for model type (iii) with the linearized calendar and linearized cyclic degradation model. The bottom of Fig. 7 depicts the development of the SOH and arbitrage profit for the identified optima over time. The results show that the more complex aging cost models allow to generate more profit, while being subjected to similar SOH trajectories, resulting in 80% SOH at the end of the investigated 12-year time horizon. Compared to aging cost model (i), the maximum profit from energy arbitrage is 24.9% higher with aging cost model (ii) and 29.3% with aging cost model (iii).

The analysis of the relevant aging stress factors in Fig. 8 highlights how this increase in cumulative profit is achieved. Including the linearized calendar and cyclic aging cost models in the optimization model, leads to an improved aging aware operation strategy. In summary, the detailed aging cost models in the optimization model entice the BESS to avoid those energy arbitrage opportunities that promise high arbitrage profit but would also cause high battery degradation. This in turn enables the BESS to complete more FECs that are less profitable but also less straining for the battery and thereby achieve a higher profit over its total lifetime.

With the linearized calendar degradation model in aging cost model (ii), the BESS is able to complete 4378.6 FECs over the 12-year time horizon before reaching its end of life, compared to 2477.8 FECs for aging cost model (i). The lower average SOC reduces calendar aging and the coincidentally slightly lower average C_{rate} and DOC cyclic aging, thereby enabling this increase in FECs before the end of life. However, the average cumulative profit per FEC decreases from 193.6 EUR with aging cost model (i) to 136.8 EUR with aging cost model (ii). This highlights that the BESS engages in more, but on average less profitable energy arbitrage opportunities with aging cost model (ii).

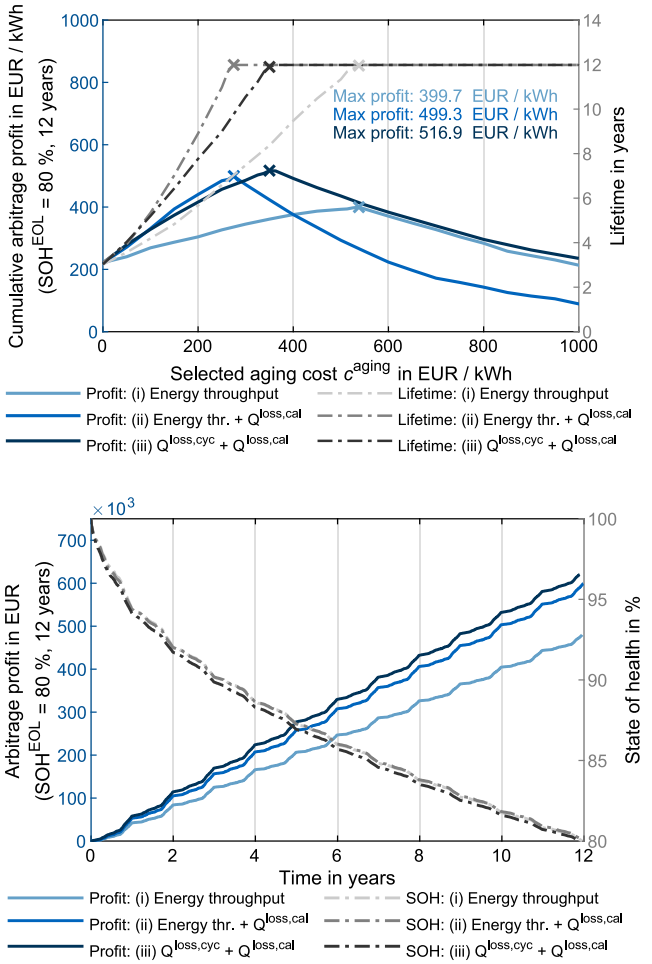

Fig. 7. Top: Cumulative profit from energy arbitrage after 12 years of operation for different aging cost values. All three aging cost models with increasing complexity are depicted here: (i) Energy throughput model, (ii) Energy throughput and calendar degradation model, (iii) Cyclic and calendar degradation model. Bottom: Arbitrage profit and SOH over time for the *optimal aging cost*: (i) c^{aging} = 538 EUR/kWh, (ii) c^{aging} = 275 EUR/kWh, (iii) c^{aging} = 350 EUR/kWh.

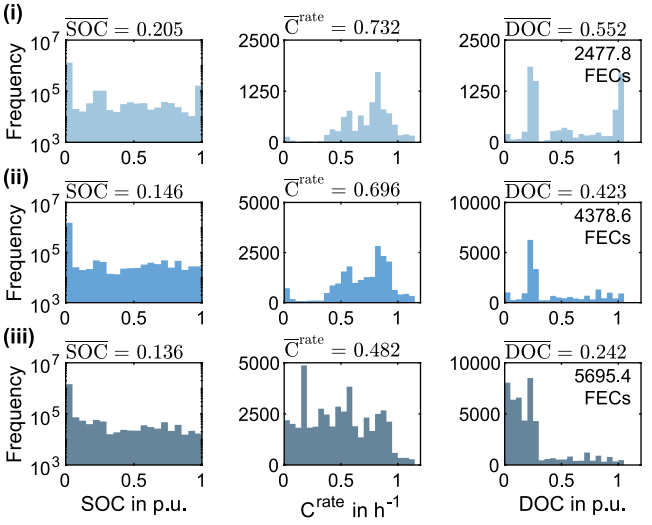

Fig. 8. Distribution of the calendar aging stress factor SOC and the cyclic aging stress factors C_{rate} and DOC for the three different aging cost models (i), (ii) and (iii) with the *optimal aging cost* from Fig. 7.

With the additional linearized cyclic degradation model in aging cost model (iii), the average SOC, C_{rate} and DOC are further reduced. Analogously to model type (ii), the largest reduction of stress factors for model type (iii) is seen in the cyclic aging stress factors C_{rate} and DOC as expected, but a slight reduction in the average SOC is seen as well. The 5695.4 FECs until the end of life translates to an average profit per FEC of 108.9 EUR.

3.3. Impact of interest rate, end-of-life threshold and price profile

After the previous sections have focused on the cumulative profit as the main financial indicator, we now investigate the net present value (NPV) of future profit. The NPV is a common financial metric to assess investment options. It discounts future profit and thereby considers that profit in earlier years is more valuable than in later years of an investment, since the earlier profit can be invested elsewhere and generate return. The NPV here is calculated as follows:

$$\mathrm{NPV} = \sum_{m=0}^{M} \frac{\mathbb{P}_m^{\mathrm{arb}}}{(1+\mathrm{i})^m} \tag{27}$$

Here, $\mathbb{P}_m^{\mathrm{arb}}$ is the cumulative profit from energy arbitrage in year m and i the interest rate.

The top of Fig. 9 shows the NPV of arbitrage profit for different aging cost values and interest rates. Furthermore, the lifetime in years is given until the EOL criterion of 80% SOH is reached for each aging cost value. Aging cost model type (i) is used here which only considers the energy throughput. The time horizon here is increased to 20 years to investigate the influence of the interest rate i on the optimal lifetime.

With an interest rate of i = 0%, the NPV simply equals the cumulative profit from energy arbitrage from the previous sections. With i = 0% and the *optimal aging cost* of 825 EUR/kWh, a cumulative profit of 444.5 EUR/kWh is reached after 20.0 years, at an average yearly profit of 26.7 kEUR. While for the 12-year time horizon with *optimal aging cost* of 538 EUR/kWh, a cumulative profit of 399.7 EUR/kWh is reached, at an average yearly profit of 40.0 kEUR. Prolonging the investigated horizon from 12 to 20 years and extending the BESS lifetime by increasing the aging cost, therefore does not lead to a proportional increase in the cumulative profit.

In the previous sections, the optimal cumulative profit was nevertheless reached when the aging cost are chosen such that the EOL is reached at the end of the investigated time horizon, i.e. 12 years. By using the NPV as the main financial metric, this relationship changes. The higher the interest rate, the lower the value of future profit. Therefore, for high interest rates, the optimal aging cost and resulting lifetime decrease, as it is beneficial to generate a higher profit in early years and forego additional profit in later years. For an interest rate of i = 7.5%, the optimal NPV of 265.9 EUR/kWh is reached if aging cost are set to 250 EUR/kWh, which results in a BESS lifetime of 8.7 years. The interest rate can therefore be the starting point for designing an aging aware operation strategy, by choosing the aging cost value that yields the optimal NPV and the resulting BESS lifetime for the relevant interest rate.

The bottom of Fig. 9 shows how different thresholds for the EOL affect the *optimal aging cost*. In general, the higher the SOH limit for the EOL threshold, the higher the aging cost should be chosen, as low aging cost would lead to a particularly early EOL in that case. The results highlight the importance of the EOL assumption for the assessment of the expected lifetime profit. The degradation model used here was validated until around 80% SOH [48,49]. Insights into the aging behavior towards the EOL, such as when an aging knee [16] can be expected, would be of use twofold. First, a more accurate assessment of the expected lifetime profit can be obtained in the planning phase of a BESS project. Second, if the aging behavior towards the EOL is known, the aging cost can be set accordingly to optimize the lifetime profit for the operation phase of a BESS project. Instead of having all information available at the beginning of a BESS project, one may choose though

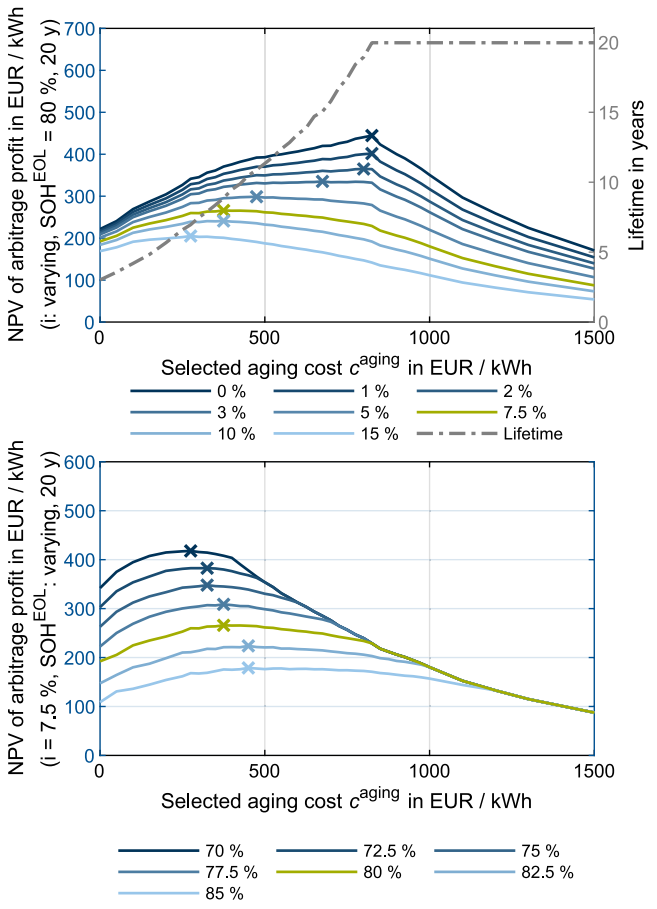

Fig. 9. NPV of arbitrage profit after 20 years of operation for different aging cost values. Aging cost model (i) was used here. The top figure shows the impact of the interest rate on the optimal definition of aging cost, while assuming a constant EOL threshold at $\mathrm{SOH}^{\mathrm{EOL}} = 80\%$. The bottom figure shows the impact of the EOL threshold while assuming a constant interest rate of i = 7.5%.

to update the aging aware operation strategy, i.e. the chosen value for the aging cost or the aging cost model itself, once more information becomes available through the analysis of field data over the years of operation.

After previously using ID-1 price data from the year 2021, Fig. 10 now shows the NPV for different aging cost values with ID-1 prices from the years 2019 to 2022. The price data was obtained from [45] as well. Table 3 summarizes the optimal values when either aiming to maximize the lifetime NPV with an interest rate of i = 7.5% or maximizing profit over a 12 year horizon. Most noticeably, the maximum lifetime NPV and profit significantly increase from 2019 to 2022. The higher maximum lifetime NPV is a consequence of the increasing electricity prices and higher electricity price volatility as shown by the mean and standard deviation of the ID-1 price index in Table 3. In addition, the more profitable energy arbitrage opportunities also lead to a higher aging cost value yielding the optimal lifetime profit. With price data from the year 2019, c^{aging} = 225 EUR/kWh leads to the optimal lifetime NPV of 109.7 EUR/kWh, while with price data from the year 2022, c^{aging} = 1150 EUR/kWh leads to the optimal lifetime NPV of 571.0 EUR/kWh.

For the investigations here, price data from the respective year was looped over the full time horizon. However, the dependence of the optimal aging cost on the price profile shows that the lifetime profitability in real applications can be increased by using a realistic prognosis of long-term future price data or by re-determining the optimal value for c^{aging} regularly over the years that a BESS is operated.

Table 3
Mean and standard deviation (SD) of the ID-1 prices for 2019 to 2022 and key simulation results (aging cost model type (i) and SOH^{EOL} = 80%) with those price profiles: *optimal aging cost* and resulting lifetime to achieve a maximum NPV (i = 7.5%), as well as *optimal aging cost* to achieve maximum profit over 12 years.

Year	Mean ID-1 €/MWh	SD ID-1 €/kWh	Max. NPV with i = 7.5%			Max. profit over 12 years	
			c^{aging} €/MWh	Max. NPV €/kWh	Lifetime years	c^{aging} €/kWh	Max. profit €/kWh
2019	37.6	22.6	225	109.7	11.9	225	168.4
2020	31.7	32.4	250	148.2	10.3	288	226.8
2021	97.2	78.4	400	265.4	9.5	538	399.8
2022	236.1	156.2	1150	571.0	11.5	1225	872.0

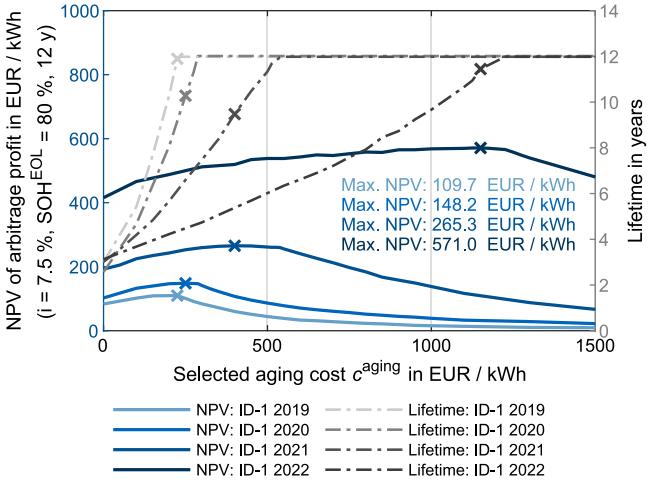

Fig. 10. NPV of arbitrage profit and lifetime after 12 years of operation for different aging cost values. Aging cost model (i) was used here. The results are depicted for the ID-1 price profiles of the years 2019 to 2022. A constant EOL threshold at SOH^{EOL} = 80% as well as an interest rate of i = 7.5% are considered for all simulations.

The results of this subsection and the previous subsection highlight that the *optimal aging cost* depends on the application (e.g. the interest rate of concern and the price profile), the aging characteristics of the BESS and the selected aging cost model. Therefore, the standard approach from literature to choose the aging cost c^{aging} based on the battery system cost (c.f. Section 1.1) leads to non-optimal lifetime profit. For example, in literature for the year 2022 values in the range of 340 to 580 USD/kWh are stated as BESS investment cost [52]. In this case study however, the *optimal aging cost* range between 225 EUR/kWh and 1225 EUR/kWh. Instead of setting the aging cost equal to the battery system cost, the here proposed MPC framework may be used to compare different optimization models and determine the *optimal aging cost* for the investigated application, thereby increasing the lifetime profitability of the BESS.

3.4. Impact of scaling aging cost and increasing lifetime profitability by accounting for the interest rate

As indicated in Section 2.3.2 and Section 2.3.3, implementing the square root dependency of calendar capacity loss on time and square root dependency of cyclic capacity loss on the number of FECs, would lead to detrimental behavior in terms of the lifetime profitability. This is highlighted in Fig. 11, which shows three different adaptions of aging cost model type (iii). The first version in light gray and light blue is with the non-scaled aging cost, which refers to including the square root dependency of cyclic and calendar capacity loss on the number of FECs and time. The second version in gray and blue is with the scaled model, which means that the linearized degradation model at $Q^{loss,cal}$ = 5% and $Q^{loss,cyc}$ = 5% is used for the optimization model, regardless of the actual total past calendar capacity loss $Q^{loss,cal}$ and total past cyclic capacity loss $Q^{loss,cyc}$ of the digital twin. This is the scenario of using the orange lines from Fig. 3 and Fig. 4, instead of

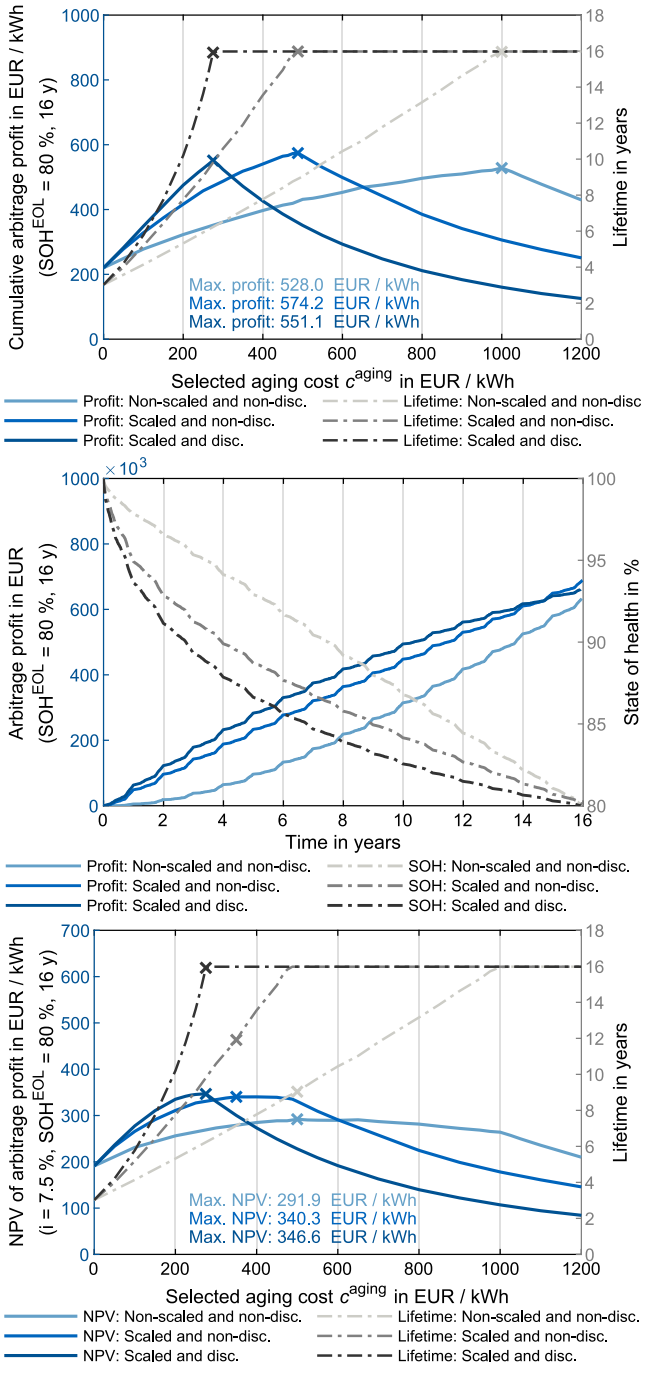

Fig. 11. Top: Cumulative arbitrage profit after 16 years of operation for different aging cost values. Here, three different adaptions for the aging cost model (iii) are investigated: non-scaled and non-discounted, scaled and non-discounted, as well as scaled and discounted. Mid: Cumulative arbitrage profit and state of health over time for the *optimal aging cost* from the top figure. Bottom: NPV of arbitrage profit for the three different adaptions of aging cost model (iii).

selecting the respective set of linearization points based on $Q^{\text{loss,cal}}$ and $Q^{\text{loss,cyc}}$ at the beginning of each optimization. It can be seen that the scaled aging cost has a beneficial effect on both the 16-year maximum cumulative profit (top plot) and the NPV (bottom plot). The maximum cumulative arbitrage profit is 8.7% higher and the maximum NPV of arbitrage profit is 16.6% higher, compared to the non-scaled scenario.

The middle plot of Fig. 11 highlights why this is the case. The square root dependency leads to over-proportionally high aging cost in the first few years, resulting in a low amount of cycling and arbitrage profit in the early years (light blue and light gray line). With non-scaled aging cost, a profit of 5.4 kEUR is achieved in year 1 and 48.9 kEUR in year 10. This higher profit in later years is subject to a higher discount rate and therefore less beneficial for the NPV, c.f. Eq. (27). With the scaled aging cost (blue and gray lines), the magnitude of aging cost remains the same throughout the years, while the impact of the stress factors SOC, C_{rate} and DOC is still considered in the aging cost model. As a result, there is a more consistent level of profit over time. In addition, the previous trend reverses, since the lower usable capacity and the higher losses due to the increasing cell resistance, cause slightly lower profits in later years. With scaled aging cost, a profit of 49.1 kEUR is achieved in year 1 and 41.7 kEUR in year 10.

The third adaption of aging cost model (iii) aims to further utilize the fact that earlier profit is more valuable in terms of the NPV. The aging cost formulation inside the optimization model is adapted as follows:

$$c^{\text{aging}'} = c^{\text{aging}} * (1+i)^m \tag{28}$$

With i being the interest rate that is used for the project evaluation, here $i = 7.5\%$ and m the current fractional year since the start of the simulation horizon. Thereby, aging cost at the end of the 16-year simulation horizon are 3.18 times higher than at the beginning, leading to more profit in earlier than in later years. By both scaling and discounting the aging cost, the maximum cumulative arbitrage profit is 4.4% higher and the maximum NPV of the arbitrage profit is 18.7% higher than for the non-scaled and non-discounted scenario. A profit of 63.3 kEUR is achieved in year 1 and 36.7 kEUR in year 10.

In summary, scaling the aging cost to $Q^{\text{loss,cal}} = 5\%$ and $Q^{\text{loss,cyc}} = 5\%$ in the scenario investigated here has a beneficial effect on both the cumulative profit from energy arbitrage and its NPV. Further discounting the aging cost leads to a lower cumulative profit but an even higher NPV, compared to only scaling the aging cost, since more profit is generated in earlier years.

4. Conclusions

With the steadily growing amount of globally installed BESSs, aging aware operation of these systems becomes increasingly relevant. Operating a BESS under consideration of the relevant aging stress factors promises higher profits over its lifetime and more resource-efficient use of battery cells. For designing and benchmarking aging aware operation strategies, this work presents a model predictive control framework. By simulating the entire lifetime on a digital twin of the BESS, different aging aware optimization models can be compared before the optimal operation strategy is deployed to the real-world BESS. This work focuses on the application of generating profit through arbitrage trading on the EPEX Spot intraday electricity market. For that purpose, a linearized MILP ready model for the calendar and cyclic capacity loss of a LFP battery cell is presented. The proposed MPC framework is made available open-source [43] and designed in a modular way, such that different use cases and optimization formulations may be added and investigated. In contrast to previous contributions, we investigate the entire lifetime with the MPC framework, which allows to quantify the effect of aging aware operation on the lifetime profitability of BESSs, including the benefit of different degrees of complexity for modeling battery aging. Furthermore, the effect of aging cost c^{aging} on lifetime profitability is investigated in detail and the MPC framework is used to determine the *optimal aging cost*.

The results show that over the same investigated 12-year time horizon, the lifetime profit from energy arbitrage can be increased by 24.9% with the linearized calendar degradation model and by 29.3% with the linearized calendar and cyclic degradation model as part of the optimization model formulation, compared to only assuming energy throughput based aging cost. The linearized degradation models entice the BESS to avoid those energy arbitrage opportunities that promise high arbitrage profit but would also cause high battery degradation. This in turn enables the BESS to complete more total FECs over its lifetime and thereby achieve the before-mentioned higher lifetime profit. The results further show that the selection of the aging cost c^{aging} significantly impacts the lifetime profit and NPV. By determining the *optimal aging cost* through parameter variation with the MPC framework, the lifetime profit and NPV can be significantly increased. Most notably, the standard practice from the literature of choosing c^{aging} based on the battery system cost would lead to sub-optimal lifetime profit. Instead, the *optimal aging cost* is dependent on the aging behavior of the system, the aging cost model used in the optimization, the price profile, EOL-criterion, as well as the interest rate of concern. Scaling the degradation model and discounting the aging cost to obtain higher profit in earlier years of operation can further increase the lifetime profitability, especially when using the NPV as the financial metric of concern. In addition, the case study with price data from 2019 to 2022 shows, that the recent increases in wholesale electricity prices and wholesale electricity price volatility directly translate into a substantial increase of the achievable lifetime profit with BESSs used for arbitrage trading.

For this work, some uncertainties and limitations are considered. In the case study, price data from the respective year was looped over the full time horizon and a degradation model was used, which does account for accelerated capacity fade towards the end-of-life. As the dependence of the optimal aging aware operation strategy on the price profile and battery aging behavior highlights, the operation strategy should be reevaluated periodically by rerunning the MPC framework, once up-to-date price forecasts and additional insights into the BESS aging behavior from field data become available throughout the course of the BESS lifetime. Furthermore, the energy arbitrage application was modeled in a simplified way for the case study. Perfect foresight of the ID-1 price was assumed, which we believe to be a conservative assumption. For real-time bidding, one may achieve higher sell and lower buy prices than the ID-1 price and may place additional bids that are compensated before execution by the BESS, which can generate additional profit. On the other hand, the profit from energy arbitrage stated here does not account for market access cost, taxes, or labor costs. In addition, using the proposed framework requires the availability of a suitable degradation model, which cell manufacturers often do not provide. However, there are some third-party providers who offer degradation prognosis for BESSs. Finally, while this contribution focuses on the impact of aging aware operation on lifetime profitability, it can be worthwhile to also quantify the ecological benefit of a widespread adoption of aging aware operation.

Funding and acknowledgment

This research is funded by the German Federal Ministry of Education and Research (BMBF) via the research project greenBattNutzung (grant number 03XP0302D) and the German Federal Ministry for Economic Affairs and Climate Action (BMWK) via the research project StorageMultiApp (grant number 03EI6081B). The projects greenBattNutzung and StorageMultiApp are both overseen by Project Management Juelich (PtJ).

CRediT authorship contribution statement

Nils Collath: Conceptualization, Investigation, Methodology, Project administration, Software, Visualization, Writing – original draft, Writing – review & editing. **Martin Cornejo:** Software, Writing – review & editing. **Veronika Engwerth:** Methodology, Writing – review & editing. **Holger Hesse:** Methodology, Writing – review & editing. **Andreas Jossen:** Funding acquisition, Supervision, Writing – review & editing.

Declaration of competing interest

The authors declare that they have no known competing financial interests or personal relationships that could have appeared to influence the work reported in this paper.

Data availability

The code for the MPC framework is available open-source under [43].

Appendix A. Degradation model linearization

The degradation model by Naumann et al. describes the total capacity loss Q^{loss} as the sum of calendar capacity loss $Q^{\text{loss,cal}}$ and cyclic capacity loss $Q^{\text{loss,cyc}}$ [48,49]:

$$Q^{\text{loss}} = q^{\text{loss,cal}}(t, \text{SOC}, T) + q^{\text{loss,cyc}}(\text{FEC}, C^{\text{rate}}, \text{DOC}) \tag{29}$$

$$Q^{\text{loss,cal}} = k_{\text{ref,T}} \cdot (c_1(\text{SOC} - 0.5)^3 + d_1) \cdot \sqrt{t} \tag{30}$$

$$Q^{\text{loss,cyc}} = (a_2 C^{\text{rate}} + b_2) \cdot (c_2(\text{DOC} - 0.6)^3 + d_2) \cdot \sqrt{\text{FEC}} \tag{31}$$

Here, t, SOC, T refer to the time, state of charge, and temperature, respectively. FEC, C^{rate} and DOC refer to the number of full equivalent cycles, the charge–discharge rate, and the depth of cycle. In Eq. (30), $k_{\text{ref,T}}$, c_1 and d_1 are fitting parameters of the calendar degradation model. In Eq. (31), a_2, b_2, c_2 and d_2 are the fitting parameters of the cyclic model.

Notably, $k_{\text{ref,T}}$ in the original model by Naumann et al. describes the dependence of calendar capacity loss on temperature with an Arrhenius equation [48]. The battery cell temperature inside a BESS depends highly on the thermal design and the heating/cooling system and control [53]. To compare the different optimization models investigated here, we make the simplification of assuming a constant cell temperature of 25 °C for both the digital twin and the optimization model. This turns $k_{\text{ref,T}}$ into a constant for the purpose of this work.

A.1. Calendar aging

To adapt Eq. (30) to varying external stress factors, the concept of virtual time t^{virtual} from [48] is implemented in **SimSES** as well. t^{virtual} is the time that would have needed to pass to reach the total past calendar capacity loss under the present stress factors and can be calculated by solving Eq. (30) for t:

$$t^{\text{virtual}} = \left(\frac{Q^{\text{loss,cal}}}{k_{\text{ref,T}} \cdot (c_1 \cdot (\text{SOC} - 0.5)^3 + d_1)}\right)^2 \tag{32}$$

The additional calendar capacity loss in the current timestep $\Delta q^{\text{loss,cal}}$ can then be calculated as follows:

$$\Delta q^{\text{loss,cal}} = k_{\text{ref,T}} \cdot (c_1(\text{SOC} - 0.5)^3 + d_1) \cdot \sqrt{t^{\text{virtual}} + \Delta t} - Q^{\text{loss,cal}} \tag{33}$$

To solve this nonlinear degradation model in a MILP, it needs to be linearized. Eq. (33) has a dependence on both the past capacity loss $Q^{\text{loss,cal}}$ as well as on SOC.

$Q^{\text{loss,cal}}$ only shows minor change over the short-term optimization horizon and can therefore be assumed as a constant for each optimization horizon. However, due to the square root dependency of calendar capacity loss on time, $\Delta q^{\text{loss,cal}}$ is significantly higher for low values of $Q^{\text{loss,cal}}$ than for high values of $Q^{\text{loss,cal}}$. Therefore, we performed linearizations of the SOC for 229 different values of $Q^{\text{loss,cal}}$, as depicted in Fig. 3. The cubic dependence of $\Delta q^{\text{loss,cal}}$ on SOC is represented by a resulting set of 10 lines for each of the 229 linearization points for $Q^{\text{loss,cal}}$. For each optimization, the corresponding set of SOC linearization points is chosen based on the total capacity loss $Q^{\text{loss,cal}}$ at the beginning of the optimization horizon. Through this method, an average relative error of less than +/−4% is achieved over all $Q^{\text{loss,cal}}$ ranges.

A.2. Cyclic aging

Analogously to the approach for calendar aging, the concept of virtual full equivalent cycles $\text{FEC}^{\text{virtual}}$ is used to apply Eq. (31) to varying external stress factors:

$$\text{FEC}^{\text{virtual}} = \left(\frac{Q^{\text{loss,cyc}}}{(a_2 C^{\text{rate}} + b_2) \cdot (c_2(\text{DOC} - 0.6)^3 + d_2)}\right)^2 \tag{34}$$

The additional degradation after a cycle is then calculated as follows:

$$\Delta q^{\text{loss,cyc}} = (a_2 C^{\text{rate}} + b_2) \cdot (c_2(\text{DOC} - 0.6)^3 + d_2) \cdot \sqrt{\text{FEC}^{\text{virtual}} + \Delta\text{FEC}} - Q^{\text{loss,cyc}} \tag{35}$$

In **SimSES**, a half-cycle counter is used which checks after every simulation steps if the charge–discharge direction has changed and then evaluates Eq. (35) with the DOC and C^{rate} from the last half-cycle. This nonlinear model requires linearization as well in order to be represented as part of a MILP. $\text{FEC}^{\text{virtual}}$ and C^{rate} are directly related for fixed timesteps and can be expressed through the energy throughput for those timesteps. However, determining the DOC would require the implementation of half-cycle counting in the scheduling method based on integer variables. Furthermore, the dependency of $\Delta q^{\text{loss,cyc}}$ on two multiplied decision variables, i.e. C^{rate} and DOC, would make the model inherently nonlinear. We therefore introduce the following simplification to linearize this cyclic degradation model: We subdivide the optimization horizon into 4 h time blocks. For each 4 h time block, the DOC is expressed through the energy throughput as well. If the DOC exceeds an increment of 100% for a given 4 h time block in either charge or discharge direction, this is evaluated as one half-cycle plus the remaining DOC as a partial cycle.

Analogously to calendar aging, $\Delta q^{\text{loss,cyc}}$ is significantly higher for low values of $Q^{\text{loss,cyc}}$ than for high values of $Q^{\text{loss,cyc}}$, due to the square root dependency of cyclic capacity loss on the number of FECs. We therefore perform the above linearization of C^{rate} and DOC in 229 points of $Q^{\text{loss,cyc}}$. Applying this principle to Eq. (35), leads to the linearized capacity loss from Fig. 4.

References

[1] Figgener J, Hecht C, Haberschusz D, Bors J, Spreuer KG, Kairies K-P, Stenzel P, Sauer DU. The development of battery storage systems in Germany: A market review (status 2023). 2022, URL http://arxiv.org/pdf/2203.06762v3.

[2] USDepartment of Energy. Energy storage grand challenge: Energy storage market report. 2020, URL https://www.energy.gov/energy-storage-grand-challenge/downloads/energy-storage-market-report-2020.

[3] Killer M, Farrokhseresht M, Paterakis NG. Implementation of large-scale Li-ion battery energy storage systems within the EMEA region. Appl Energy 2020;260:114166. http://dx.doi.org/10.1016/j.apenergy.2019.114166.

[4] USEnergy Information Administration. Battery storage in the United States: An update on market trends. 2020, URL https://www.eia.gov/analysis/studies/electricity/batterystorage/,

[5] Vetter J, Novák P, Wagner MR, Veit C, Möller K-C, Besenhard JO, Winter M, Wohlfahrt-Mehrens M, Vogler C, Hammouche A. Ageing mechanisms in lithium-ion batteries. J Power Sources 2005;147:269–81. http://dx.doi.org/10.1016/j.jpowsour.2005.01.006.

[6] Han X, Lu L, Zheng Y, Feng X, Li Z, Li J, Ouyang M. A review on the key issues of the lithium ion battery degradation among the whole life cycle. ETransportation 2019. http://dx.doi.org/10.1016/j.etran.2019.100005.

[7] Edge JS, O'Kane S, Prosser R, Kirkaldy ND, Patel AN, Hales A, Ghosh A, Ai W, Chen J, Yang J, Li S, Pang M-C, Bravo Diaz L, Tomaszewska A, Marzook MW, Radhakrishnan KN, Wang H, Patel Y, Wu B, Offer GJ. Lithium ion battery degradation: what you need to know. Phys Chem Chem Phys PCCP 2021;23(14):8200–21. http://dx.doi.org/10.1039/d1cp00359c.

[8] Uddin K, Gough R, Radcliffe J, Marco J, Jennings P. Techno-economic analysis of the viability of residential photovoltaic systems using lithium-ion batteries for energy storage in the United Kingdom. Appl Energy 2017;206(10):12–21. http://dx.doi.org/10.1016/j.apenergy.2017.08.170.

[9] Wankmüller F, Thimmapuram PR, Gallagher KG, Botterud A. Impact of battery degradation on energy arbitrage revenue of grid-level energy storage. J Energy Storage 2017;10(11):56–66. http://dx.doi.org/10.1016/j.est.2016.12.004.

[10] Collath N, Gasper P, Jossen A, Smith K, Hesse H. The economic impact of battery degradation modelling uncertainty. In: IEEE, editor. 2022 IEEE Power & Energy Society General Meeting. PESGM, 2022, http://dx.doi.org/10.1109/PESGM48719.2022.9916844.

[11] Hou Q, Yu Y, Du E, He H, Zhang N, Kang C, Liu G, Zhu H. Embedding scrapping criterion and degradation model in optimal operation of peak-shaving lithium-ion battery energy storage. Appl Energy 2020;278:115601. http://dx.doi.org/10.1016/j.apenergy.2020.115601.

[12] Cai J, Zhang H, Jin X. Aging-aware predictive control of PV-battery assets in buildings. Appl Energy 2019;236:478–88. http://dx.doi.org/10.1016/j.apenergy.2018.12.003.

[13] Engels J, Claessens B, Deconinck G. Techno-economic analysis and optimal control of battery storage for frequency control services, applied to the german market. Appl Energy 2019;242:1036–49. http://dx.doi.org/10.1016/j.apenergy.2019.03.128.

[14] Weitzel T, Schneider M, Glock CH, Löber F, Rinderknecht S. Operating a storage-augmented hybrid microgrid considering battery aging costs. J Clean Prod 2018;188(7):638–54. http://dx.doi.org/10.1016/j.jclepro.2018.03.296.

[15] Kruger E, Tran QT. Minimal aging operating strategies for battery energy storage systems in photovoltaic applications. In: 2016 IEEE PES Innovative Smart Grid Technologies Conference Europe (ISGT-Europe). IEEE; 2016, p. 1–6. http://dx.doi.org/10.1109/ISGTEurope.2016.7856325.

[16] Attia PM, Bills A, Brosa Planella F, Dechent P, dos Reis G, Dubarry M, Gasper P, Gilchrist R, Greenbank S, Howey D, Liu O, Khoo E, Preger Y, Soni A, Sripad S, Stefanopoulou AG, Sulzer V. Review—"Knees" in lithium-ion battery aging trajectories. J Electrochem Soc 2022;169(6):060517. http://dx.doi.org/10.1149/1945-7111/ac6d13.

[17] Keil J, Jossen A. Electrochemical modeling of linear and nonlinear aging of lithium-ion cells. J Electrochem Soc 2020;167(11):110535. http://dx.doi.org/10.1149/1945-7111/aba44f.

[18] Fermín-Cueto P, McTurk E, Allerhand M, Medina-Lopez E, Anjos MF, Sylvester J, dos Reis G. Identification and machine learning prediction of knee-point and knee-onset in capacity degradation curves of lithium-ion cells. Energy AI 2020;1(5):100006. http://dx.doi.org/10.1016/j.egyai.2020.100006.

[19] Collath N, Tepe B, Englberger S, Jossen A, Hesse H. Aging aware operation of lithium-ion battery energy storage systems: A review. J Energy Storage 2022;55(11):105634. http://dx.doi.org/10.1016/j.est.2022.105634.

[20] Schmalstieg J, Käbitz S, Ecker M, Sauer DU. A holistic aging model for Li(NiMnCo)O2 based 18650 lithium-ion batteries. J Power Sources 2014;257:325–34. http://dx.doi.org/10.1016/j.jpowsour.2014.02.012.

[21] Sarasketa-Zabala E, Gandiaga I, Rodriguez-Martinez LM, Villarreal I. Calendar ageing analysis of a LiFePO4/graphite cell with dynamic model validations: Towards realistic lifetime predictions. J Power Sources 2014;272:45–57. http://dx.doi.org/10.1016/j.jpowsour.2014.08.051.

[22] Guenther C, Schott B, Hennings W, Waldowski P, Danzer MA. Model-based investigation of electric vehicle battery aging by means of vehicle-to-grid scenario simulations. J Power Sources 2013;239:604–10. http://dx.doi.org/10.1016/j.jpowsour.2013.02.041.

[23] Schimpe M, Kuepach MEv, Naumann M, Hesse H, Smith K, Jossen A. Comprehensive modeling of temperature-dependent degradation mechanisms in lithium iron phosphate batteries. J Electrochem Soc 2018;165(2):A181–93. http://dx.doi.org/10.1149/2.1181714jes.

[24] Angenendt G, Zurmühlen S, Axelsen H, Sauer DU. Comparison of different operation strategies for PV battery home storage systems including forecast-based operation strategies. Appl Energy 2018;229(1):884–99. http://dx.doi.org/10.1016/j.apenergy.2018.08.058.

[25] Weitzel T, Glock CH. Energy management for stationary electric energy storage systems: A systematic literature review. European J Oper Res 2018;264(2):582–606. http://dx.doi.org/10.1016/j.ejor.2017.06.052.

[26] Yang Z, Li K, Foley A. Computational scheduling methods for integrating plug-in electric vehicles with power systems: A review. Renew Sustain Energy Rev 2015;51:396–416. http://dx.doi.org/10.1016/j.rser.2015.06.007.

[27] Reniers JM, Mulder G, Ober-Blöbaum S, Howey DA. Improving optimal control of grid-connected lithium-ion batteries through more accurate battery and degradation modelling. J Power Sources 2018;379:91–102. http://dx.doi.org/10.1016/j.jpowsour.2018.01.004.

[28] Hesse H, Kumtepeli V, Schimpe M, Reniers J, Howey D, Tripathi A, Wang Y, Jossen A. Ageing and efficiency aware battery dispatch for arbitrage markets using mixed integer linear programming. Energies 2019;12(6):999. http://dx.doi.org/10.3390/en12060999.

[29] Schimpe M, Barreras J, Wu B, Offer GJ. Battery degradation-aware current derating: An effective method to prolong lifetime and ease thermal management. J Electrochem Soc 2021;168. http://dx.doi.org/10.1149/1945-7111/ac0553.

[30] Shi Y, Xu B, Tan Y, Kirschen D, Zhang B. Optimal battery control under cycle aging mechanisms in pay for performance settings. IEEE Trans Automat Control 2019;64(6):2324–39. http://dx.doi.org/10.1109/TAC.2018.2867507.

[31] Padmanabhan N, Ahmed M, Bhattacharya K. Battery energy storage systems in energy and reserve markets. IEEE Trans Power Syst 2020;35(1):215–26. http://dx.doi.org/10.1109/TPWRS.2019.2936131.

[32] Shi Y, Xu B, Wang D, Zhang B. Using battery storage for peak shaving and frequency regulation: Joint optimization for superlinear gains. IEEE Trans Power Syst 2018;33(3):2882–94. http://dx.doi.org/10.1109/TPWRS.2017.2749512.

[33] Kim W-W, Shin J-S, Kim S-Y, Kim J-O. Operation scheduling for an energy storage system considering reliability and aging. Energy 2017;141:389–97. http://dx.doi.org/10.1016/j.energy.2017.09.091.

[34] Englberger S, Jossen A, Hesse H. Unlocking the potential of battery storage with the dynamic stacking of multiple applications. Cell Rep Phys Sci 2020;1(11):100238. http://dx.doi.org/10.1016/j.xcrp.2020.100238.

[35] Hossain MA, Pota HR, Squartini S, Zaman F, Guerrero JM. Energy scheduling of community microgrid with battery cost using particle swarm optimisation. Appl Energy 2019;254(9):113723. http://dx.doi.org/10.1016/j.apenergy.2019.113723.

[36] Zia MF, Elbouchikhi E, Benbouzid M. Optimal operational planning of scalable DC microgrid with demand response, islanding, and battery degradation cost considerations. Appl Energy 2019;237:695–707. http://dx.doi.org/10.1016/j.apenergy.2019.01.040.

[37] Kazemi M, Zareipour H. Long-term scheduling of battery storage systems in energy and regulation markets considering battery's lifespan. IEEE Trans Smart Grid 2018;9(6):6840–9. http://dx.doi.org/10.1109/TSG.2017.2724919.

[38] Cao J, Harrold D, Fan Z, Morstyn T, Healey D, Li K. Deep reinforcement learning-based energy storage arbitrage with accurate lithium-ion battery degradation model. IEEE Trans Smart Grid 2020;11(5):4513–21. http://dx.doi.org/10.1109/TSG.2020.2986333.

[39] Kumtepeli V, Hesse HC, Schimpe M, Tripathi A, Wang Y, Jossen A. Energy arbitrage optimization with battery storage: 3D-MILP for electro-thermal performance and semi-empirical aging models. IEEE Access 2020;8:204325–41. http://dx.doi.org/10.1109/ACCESS.2020.3035504.

[40] Steriotis K, Sepetanc K, Smpoukis K, Efthymiopoulos N, Makris P, Varvarigos E, Pandzic H. Stacked revenues maximization of distributed battery storage units via emerging flexibility markets. IEEE Trans Sustain Energy 2022;13(1):464–78. http://dx.doi.org/10.1109/TSTE.2021.3117313.

[41] Maheshwari A, Paterakis NG, Santarelli M, Gibescu M. Optimizing the operation of energy storage using a non-linear lithium-ion battery degradation model. Appl Energy 2020;261(4):114360. http://dx.doi.org/10.1016/j.apenergy.2019.114360.

[42] He G, Ciez R, Moutis P, Kar S, Whitacre JF. The economic end of life of electrochemical energy storage. Appl Energy 2020;273:115151. http://dx.doi.org/10.1016/j.apenergy.2020.115151.

[43] Collath N. Aging_aware_MPC: Chair of electrical energy storage technology. 2023, URL https://gitlab.lrz.de/open-ees-ses/aging-aware-MPC.

[44] Möller M, Kucevic D, Collath N, Parlikar A, Dotzauer P, Tepe B, Englberger S, Jossen A, Hesse H. Simses: A holistic simulation framework for modeling and analyzing stationary energy storage systems. J Energy Storage 2022;49(11):103743. http://dx.doi.org/10.1016/j.est.2021.103743.

[45] Fraunhofer Institute for Solar Energy Systems. Energy charts. 2022, URL https://www.energy-charts.info/?l=en&c=DE.

[46] EPEX Spot. EPEX spot indices. 2023, URL https://www.epexspot.com/en/indices.

[47] Draheim P, Schlachter U, Wigger H, Worschech A, Brand U, Diekmann T, Schuldt F, Hanke B, von Maydell K, Vogt T. Business case analysis of hybrid systems consisting of battery storage and power-to-heat on the German energy market. Utilities Policy 2020;67(2):101110. http://dx.doi.org/10.1016/j.jup.2020.101110.

[48] Naumann M, Schimpe M, Keil P, Hesse HC, Jossen A. Analysis and modeling of calendar aging of a commercial LiFePO4/graphite cell. J Energy Storage 2018;17:153–69. http://dx.doi.org/10.1016/j.est.2018.01.019.

[49] Naumann M, Spingler FB, Jossen A. Analysis and modeling of cycle aging of a commercial LiFePO4/graphite cell. J Power Sources 2020;451:227666. http://dx.doi.org/10.1016/j.jpowsour.2019.227666.

[50] Notton G, Lazarov V, Stoyanov L. Optimal sizing of a grid-connected PV system for various PV module technologies and inclinations, inverter efficiency characteristics and locations. Renew Energy 2010;35(2):541–54. http://dx.doi.org/10.1016/j.renene.2009.07.013.

[51] Gasper P, Gering K, Dufek E, Smith K. Challenging practices of algebraic battery life models through statistical validation and model identification via machine-learning. J Electrochem Soc 2021;168:020502. http://dx.doi.org/10.1149/1945-7111/abdde1.

[52] Kucevic D, Meißner R, Jossen A, Hesse H. Battery energy storage systems as an alternative to conventional grid reinforcement. In: Energy proceedings, vol. 24. 2021, http://dx.doi.org/10.46855/energy-proceedings-9834.

[53] Schimpe M, Naumann M, Truong N, Hesse HC, Santhanagopalan S, Saxon A, Jossen A. Energy efficiency evaluation of a stationary lithium-ion battery container storage system via electro-thermal modeling and detailed component analysis. Appl Energy 2018;210(4):211–29. http://dx.doi.org/10.1016/j.apenergy.2017.10.129.